

Magnetic separation of elastin-like polypeptide receptors for enrichment of cellular and molecular targets

Duy Tien Ta^{1,2}, Rosario Vanella^{1,2}, Michael A. Nash^{1,2,}*

¹ Department of Chemistry, University of Basel, 4058 Basel, Switzerland

² Department of Biosystems Science and Engineering, Swiss Federal Institute of Technology
(ETH Zurich), 4058 Basel, Switzerland

Corresponding Authors

*E-mail: michael.nash@unibas.ch

Tel: +41 61 207 38 44

ABSTRACT

Protein-conjugated magnetic nanoparticles (mNPs) are promising tools for a variety of biomedical applications, from immunoassays and biosensors to theranostics and drug-delivery. In such applications, conjugation of affinity proteins (e.g., antibodies) to the nanoparticle surface many times compromises biological activity and specificity, leading to increased reagent consumption and decreased assay performance. To address this problem, we engineered a biomolecular magnetic separation system that eliminates the need to chemically modify the capture biomolecules with nanoparticles or synthetic polymers of any kind. The system consists of (i) thermo-responsive magnetic iron oxide nanoparticles displaying poly(N-isopropylacrylamide) (pNIPAm), and (ii) an elastin-like polypeptide (ELP) fused with the affinity protein Cohesin (Coh). Proper design of pNIPAm-mNPs and ELP-Coh allowed for efficient cross-aggregation of the two distinct nanoparticle types under collapsing stimuli, which enabled magnetic separation of ELP-Coh aggregates bound to target Dockerin (Doc) molecules. Selective re-solubilization of the ELP-Coh:Doc complexes was achieved under intermediate conditions under which only the pNIPAm-mNPs remained aggregated. We show that ELP-Coh is capable of magnetically separating and purifying nanomolar quantities of Doc as well as eukaryotic whole cells displaying the complementary Doc domain from diluted human plasma. This modular system provides magnetic enrichment and purification of captured molecular targets, and eliminates the requirement of bio-functionalization of magnetic nanoparticles to achieve bioseparations. Our streamlined and simplified approach is amenable for point-of-use applications and brings the advantages of ELP-fusion proteins to the realm of magnetic particle separation systems.

KEY WORDS: ELP, cross-aggregation, magnetic nanoparticle, molecule/cell capture, pNIPAm.

Interdisciplinary efforts in the fields of protein engineering, nanomaterials, and polymer chemistry are advancing bioseparation technology in ways not previously thought possible. New compositions of stimuli-responsive polymers, nanoparticles and proteins are being rationally designed to perform precise tasks and directed interactions inside complex biological fluids. Both magnetic nanoparticles¹⁻⁶ and stimuli-responsive polymers have proven extremely useful independently, as well as in combination⁵⁻¹¹ for the separation of biomolecules and cells from blood, saliva and urine for use in biosensors, and immunoassay systems.

When designing separation systems for bioassays, it is important to acknowledge the inherent trade off between the size of the capture reagents, and the mechanisms by which they can be separated from biological fluids. Several factors can be considered when rating the performance of a biological separation system. The size of reagents, their tendency to undergo non-specific interactions with sample matrix components, and their diffusivity all have strong effects on assay performance. These performance parameters can be evaluated to determine how to optimize features such as the speed of separation, efficiency, sensitivity and specificity for a given application.

Magnetic particles are straightforward to separate using simple rare earth magnets¹²⁻¹⁶. When affinity biomolecules such as antibodies or oligonucleotides are conjugated to magnetic nanoparticles and bound to their targets, a magnetic force applied to the nanoparticle is transmitted through the chemical linkages of the polymer tether/antibody, and exerted along the non-covalent binding interface to the target. By such means, protein targets are subjected to magnetic forces which actuate them within a liquid medium against Brownian forces. This separation mechanism has created an interest in bioconjugate techniques to immobilize capture biomolecules onto the surfaces of magnetic particles.¹⁷ However, in many cases, immobilization of biomolecules onto

nanoparticle surfaces can compromise binding activity,^{18,19} especially in the case of chemical conjugation to particles in which random immobilization might result in interference with the active site and/or hindering its accessibility to the analytes.²⁰ Van Leemputten and Horisberger²¹ and Kazenwadel et al.²² reported that coupling of enzymes (trypsin, glucose oxidase, horseradish peroxidase, etc) onto magnetic particles resulted in significant activity loss down to 35-0.1%, depending on the particle to enzyme ratios used. Immobilization of antibodies also was found to decrease their binding activity from slight reduction to complete loss, depending on the methods used.^{23,24} In general, the immobilization of proteins onto nanoparticle surfaces inhibits bioactivity, is time- and labor-consuming, and cost intensive.

Magnetic separation of small microparticles on the order of hundreds of nanometers to micrometers can be achieved rapidly in seconds. Such particles, however, exhibit lower specific surface area to volume ratios than smaller nanoparticles on the order of 10 nm, which lowers the binding capacity per gram. Larger particles also require longer to reach equilibrium and may not bind bulky targets (e.g., large proteins and cells) as compared with small nanoparticles due to significant steric hindrance. Alternatively, small nanoparticles on the order of 10s of nanometers will bind bulky targets with essentially diffusion-limited reaction rates, and reach equilibrium quickly. The challenge, however, is that 10 nm particles are difficult to magnetically separate because thermal Brownian forces overwhelm the magnetic forces which scale with the particle volume. This inherent paradox for magnetic separation systems has created a strong need for systems that can combine the rapid binding kinetics of small molecular-scale capture reagents with the ease of rapid separation in a modest magnetic field.

Stimuli-responsive polymers have also played an important role in bioseparations. Bio-conjugated poly(N-isopropylacrylamide),²⁵⁻²⁹ poly(oligoethylene glycol),^{30,31} and elastin-like

polypeptides,³² for example, have all been utilized as capture reagents for thermo-precipitation and biosensing.^{33–35} Separation is achieved by raising the sample temperature above the lower critical solution temperature (LCST) to create insoluble polymer aggregates, which can be separated using a centrifugal field. Such systems can achieve sensitive detection of biomarkers, however, the requirement of centrifugal fields may be limiting in certain settings. For resource limited settings, ideally a testing system could be administered without the need for a central lab facility or even electricity, eliminating the possibility of using centrifugal fields. Therefore, in specific applications magnetic particles are highly advantageous because they can be separated without requiring a centrifuge.

Elastin-like polypeptides (ELPs) are biological protein polymers consisting of repetitive (VPGXG)_n sequences, where X comprises any natural guest amino acid residue excluding proline. Like their synthetic smart polymer counterparts, ELPs show LCST behavior with the added benefit of being programmed at the genetic level and therefore completely monodisperse. Another advantage of ELP systems is the ability to genetically fuse ELP-tags to a protein of interest through a cleavable linker.³⁶ The fusion domain can be thermo-precipitated from a sample fluid and cleaved from the ELP, or bound to a specific target to achieve affinity separation. This separation mechanism, however, suffers from the same limitations as synthetic polymer thermo-precipitation systems by requiring a centrifugal field. Although filtration membranes can in principle work, volumetric throughput is limited in such systems.³⁴

Here we sought to combine the advantages of ELP-fusion proteins with the ease of magnetic particle separations. Our system addresses several of the existing limitations of bioseparation technologies by demonstrating the cross-aggregation of pNIPAm-mNPs with ELPs, followed by magnetic separation of the co-entrained ELPs. This simple yet effective strategy enabled rapid

magnetic enrichment of molecular and cellular targets that were bound to ELP-receptor fusions. Our approach eliminates the need to modify the magnetic particles with capture biomolecules, and extends the advantages of ELPs into the realm of magnetic targeting and bioseparations.

To design an effective magnetic capture system for ELPs, we produced mNPs decorated with a 10 kDa pNIPAm containing a dodecyl hydrocarbon tail and a terminal carboxyl group. We synthesized these polymers via RAFT polymerization, and used them as colloidal stabilizing agents for iron oxide particle synthesis through thermal decomposition of iron pentacarbonyl. The resulting mNP morphology was characterized by TEM (Figure 1A), with particle diameters of ~10 nm, consistent with previous reports.^{5,6,8,9} The thermally-responsive pNIPAm chains remained on the crystalline nanoparticle surface following purification by dialysis. Raising the temperature above the LCST of pNIPAm resulted in aggregation of the mNPs and clouding up of the solution. In the presence of a strong magnet below the LCST, the mNPs were found to be non-responsive on a timescale of 30 min. Upon raising the temperature above the LCST or upon addition of salt, mNP aggregates were rapidly formed and magnetophoresed to the side of the reaction vessel on a timescale of 1 minute. This property of aggregation-dependent magnetophoresis served for us as inspiration for a new approach to bioseparations, whereby other polymers from solution (free polymers) could be entrained within magnetic particle aggregates.

For our capture-and-release system to function properly, it was necessary to have an orthogonal stimulus to control the aggregation properties of one particle type in relation to the other. By incorporating pH-responsive glutamate into 20% of the guest residue positions of the ELP (see full sequences in Supporting Information), we could use buffer pH-switching to easily raise and lower the LCST of the ELP conjugates. The pNIPAm chains on the mNPs each contained a single carboxyl group which responds only very weakly to pH. This difference in the pH-dependent

aggregation profiles was used to release the ELP conjugates while keeping the mNPs collapsed in the second step of the assay. The final ELP guest residue composition used for this work was (M₁V₇E₂) repeated either 9 or 12 times.

As a fusion partner for the ELP, we selected the second Cohesin (Coh) domain from scaffold A of the cellulolytic complex from *Clostridium thermocellum*. This domain is known to be very stable and binds with high affinity to many different type-I Dockerin (Doc) domains with K_D values of ~1-10 nM.³⁷⁻⁴⁰ The Docs themselves are short 8-kDa calcium-binding domains that fold into a duplicated F-hand motif. With a length of ~75 amino acids and ~2 nm folded size, Doc domains are suitable for incorporation as affinity tags when fused with fluorescent protein domains, or in cellular display systems as described below.

Sub-cloning of the gene for Cohesin at the C-terminus of the (M₁V₇E₂)₉ and (M₁V₇E₂)₁₂ ELP genes, followed by over expression in *E. coli* yielded ~25 mg of ELP-Coh fusion proteins per liter of *E. coli* culture, which were purified via a non-chromatographic inverse transition cycle purification protocol. Protein characterization was performed using gel electrophoresis and size exclusion chromatography as shown in Figure S2, Supporting Information.

The cloud point curves for the mNPs, (M₁V₇E₂)₉-Coh, and (M₁V₇E₂)₁₂-Coh (Figures 1B and 1C) demonstrate the mechanism by which coordinated or differential magnetic actuation of the pNIPAm-mNPs/ELP-Coh system could be achieved depending on the environmental stimuli. Increasing the ionic strength by addition of NaCl shifted the LCST to lower temperatures (Figure 1C) uniformly for both the ELP-Cohs and pNIPAm-mNPs, whereas lowering the pH only shifted the LCST of ELP-Coh. As shown in Figure 1B, at neutral pH ELP-Coh had an LCST of >60 °C, whereas pNIPAm-mNPs exhibited an LCST of <50 °C. Meanwhile, dropping the pH to 4.5 protonated the glutamic acid guest residues and decreased the electrostatic repulsion of ELP-Coh,

reducing the LCST to $< C$ to a point where they could be co-collapsed with pNIPAm-mNPs. Thus, the combined stimulus of pH 4.5 and 0.5 M NaCl in 20 mM acetate buffer was found to be effective for co-collapse of pNIPAm-mNPs and ELP-Coh. The design of the materials was critical in this case for achieving conditions for co-collapse of pNIPAm-mNPs and ELP-Coh that was not overly harsh so as to disrupt the Coh protein structure, inhibit binding interactions, or in the case of cell separation (see below) harm cell viability. In addition to providing molecular specificity, ELP-Coh also served as a 'free' polymer to enhance the aggregation process, as was previously reported for pNIPAm-coated gold nanoparticles.⁴¹ The co-aggregation of the pNIPAm-mNPs and ELP is based on hydrophobic interactions. On one hand, at low pH the glutamic acid residues of the ELP and the end-carboxyl groups of the pNIPAm become protonated, which decreases electrostatic repulsion between the two smart polymer types in collapsing buffer. On the other hand, the 'salting-out' effect at high NaCl concentration remarkably reduces the protein and pNIPAm solubility, leading to hydrophobic collapse and coordinated aggregation of pNIPAm and ELPs.

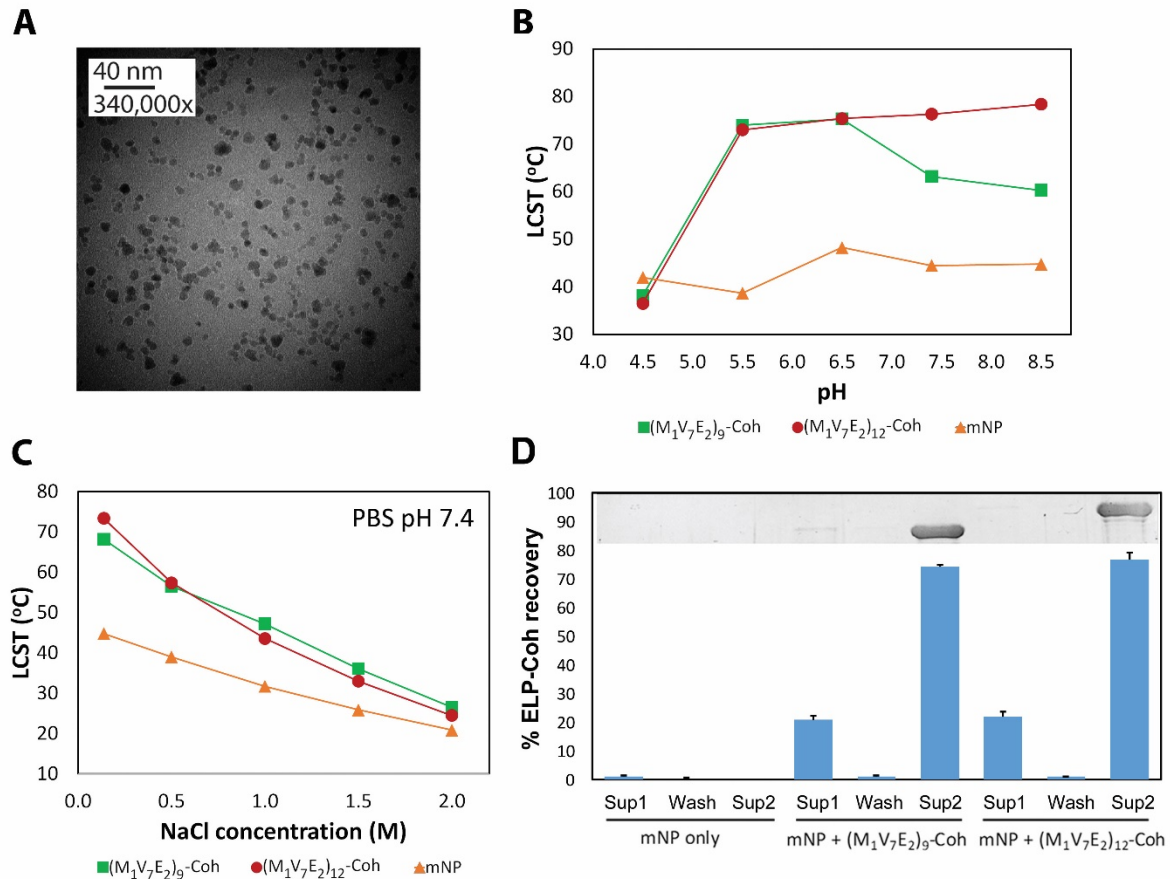


Figure 1. (A) TEM image of pNIPAm-mNPs. (B) Cloud-point assay showing responsive characteristics of pNIPAm-mNPs and ELP-Coh upon changes in pH. (C) Cloud-point assay showing responsive characteristics of pNIPAm-mNPs and ELP-Coh upon changes in salt concentration. (D) Protein quantification during co-collapse, washing, and release of the pNIPAm-mNPs and ELP-Coh. The non-captured, washed, and released supernatants were collected in ‘Sup1’, ‘Wash’ and ‘Sup2’ fractions, respectively. The protein contents of each fraction was determined by BCA assay and normalized to the initial ELP-Coh quantity (0.5 mg). SDS-PAGE analysis of each fraction is displayed on top.

In contrast to the mNPs, ELP-Coh remained soluble at 40 °C in PBS pH 7.4 containing 0.5 M NaCl, while the mNPs remained aggregated. The releasing buffer at 40 °C pH 7.4 was therefore used for recovery of soluble ELP-Coh from aggregated pNIPAm-mNPs.

To test the ability of smart magnetic nanoparticles to co-aggregate with ELPs and affect magnetic actuation of proteins, a pNIPAm-mNPs and ELP-Coh mixture was collapsed at 40°C in collapsing buffer and magnetically separated for ~1 min. We found that approximately 75% of the ELP-Coh proteins could be co-collapsed with pNIPAm-mNPs and recovered in soluble form as determined by BCA assay (Figure 1D). We found no significant differences in magnetic separation characteristics between (M₁V₇E₂)₉-Coh and (M₁V₇E₂)₁₂-Coh, and so only the (M₁V₇E₂)₉-Coh was used for further biomolecule and whole cell capture experiments as described below.

As a model biomarker, we produced and purified a fusion protein of the fluorescent iLOV domain⁴² and a type-I Dockerin module (iLOV-Doc). Binding of the engineered ELP-Coh to the fluorescent iLOV-Doc was firstly confirmed by size-exclusion chromatography (SEC) (Figure S2, Supporting Information). We then challenged the mixture of pNIPAm-mNPs and ELP-Coh with fishing out iLOV-Doc (Figure 2A) from clean buffers, 20 µg/ml BSA-buffer solutions, and 10% human plasma samples (Figure 3) while tracking the capture efficiency by measuring the fluorescence intensity. In clean buffers, a simple procedure involving co-collapse of the pNIPAm-mNPs and the ELP-Coh:iLOV-Doc complexes followed by application of a magnetic field was able to capture a majority (~85 - 90%) of iLOV-Doc in a 5 µM solution. The captured aggregate was then re-solubilized with releasing buffer (fraction 'Sup2'), resulting in an overall capture-and-release efficiency of ~75% (Figure 2B). In contrast, we used Coh-iLOV as a negative control and found that it could not be efficiently separated by the pNIPAm-mNPs and ELP-Coh mixture, appearing in the 'Sup1' non-captured fraction (Figure 2B). We note that the sum of fluorescent

intensities of all three fractions (Sup1, Wash, Sup2) from each treatment in which iLOV-Doc or Coh-iLOV was mixed with the ELP-Coh and/or mNPs was slightly lower than the total fluorescent intensity of pure iLOV-Doc or Coh-iLOV (Figure S5, Supporting information) treated with the same 40 °C collapsing buffer. This may be due to fluorescence quenching effects of iLOV-Doc inside the aggregates. This effect served to lower our observed capture efficiency, therefore our reported capture efficiencies should be considered a lower bound.

The fluorescent data of captured iLOV-Doc was in accordance with SDS-PAGE result (Figure 2C). Without pNIPAm-mNPs, the ELP-Coh:iLOV-Doc complexes could still be collapsed, however, they were not captured by the magnetic field and thus were removed in the ‘Sup1’ non-captured fraction. In addition, solutions with initially low concentrations of iLOV-Doc could significantly be enriched by resuspending the captured aggregates into smaller volumes of releasing buffer. When proteins such as BSA were spiked into the initial samples together with iLOV-Doc, magnetic separation of ELP-Coh:iLOV-Doc successfully depleted a majority of the nonspecific background proteins (Figure 2D and 2E). Notably, a collapsing and separation time as short as 1 min was sufficient for effective capture of iLOV-Doc.

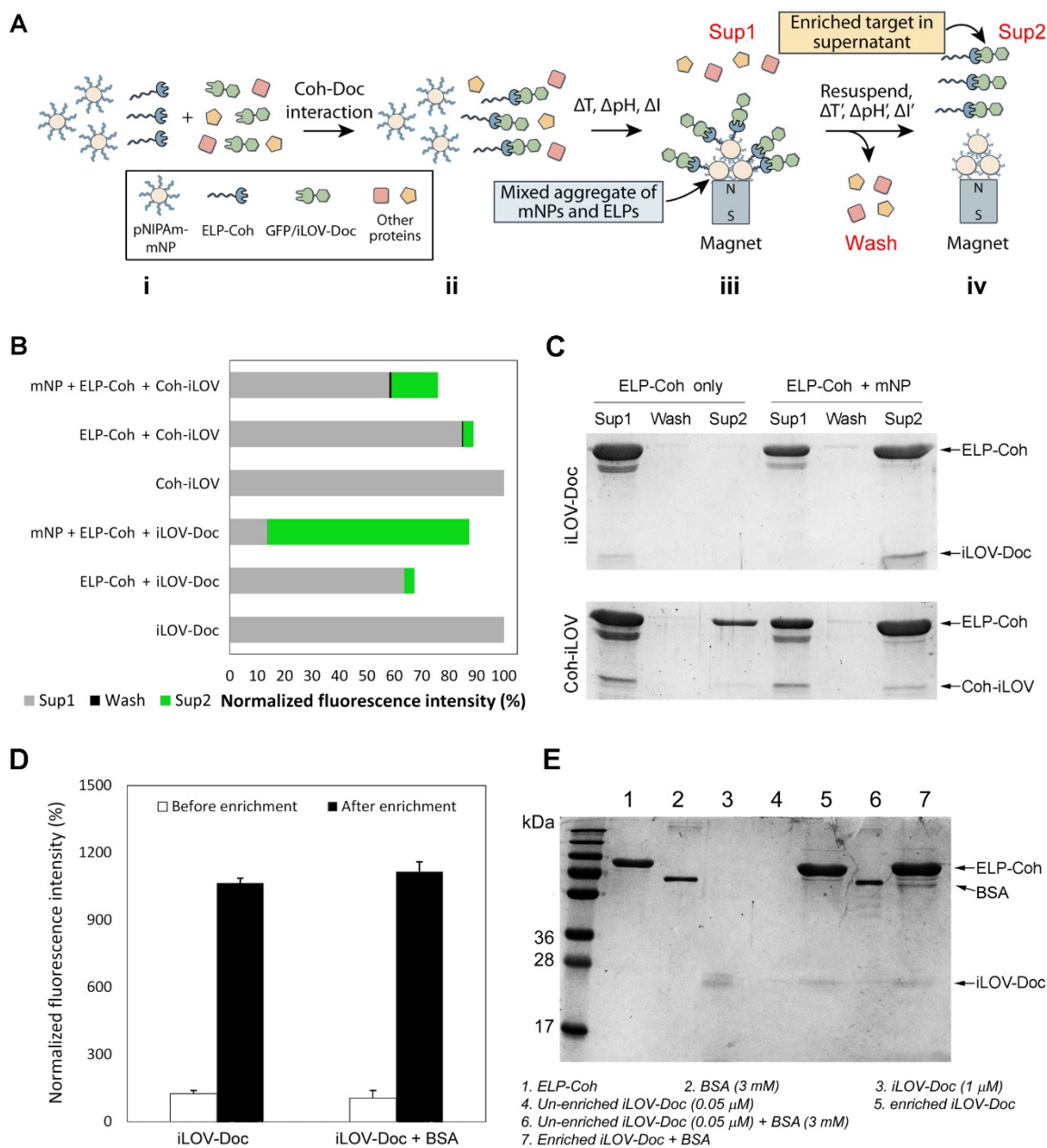


Figure 2. Magnetic separation of iLOV-Doc by ELP-Coh and pNIPAm-mNPs. **(A)** Scheme depicting reagent system for specific capture and magnetic separation of iLOV-Doc. The magnetophoretic procedure has four steps: i) pNIPAm-mNPs and ELP-Coh are mixed in a fluid containing the target (iLOV-Doc) and background proteins; ii) the ELP-Coh specifically binds iLOV-Doc in the mixture, forming ELP-Coh:iLOV-Doc complexes; iii) co-collapse of pNIPAm-mNPs and ELP-Coh occurs upon application of temperature, pH, and/or ionic stimuli. A magnet

placed against the side of the reaction vessel separates ELP-Coh:iLOV-Doc complexes together with pNIPAm-mNPs; iv) Reversal of the stimulus releases only the ELP-Coh:iLOV-Doc complexes whilst keeping the pNIPAm-mNPs collapsed. **(B)** Relative fluorescence of the non-captured fraction (Sup1), washed fraction (Wash), and released fraction (Sup2) under different treatment conditions. Fluorescence was normalized to the sample containing pure iLOV-Doc (5 μ M). Coh-iLOV was used as a non-binding control. **(C)** SDS-PAGE profiles of protein fractions displayed in **(B)**. **(D)** Enrichment of 0.05 μ M iLov-Doc by combining five captured fractions into a single aliquot of release buffer. **(E)** SDS-PAGE analysis of samples before and after enrichment. Pure ELP-Coh, iLOV-Doc and BSA were loaded as controls.

Capture of iLOV-Doc in diluted plasma was performed similarly with some modification to the collapsing conditions. Since Ca^{2+} is required for correct folding of the Doc domain, additional Ca^{2+} (5 mM) was supplemented for all experiments performed in 10% plasma to compensate for the loss of these ions due to an abundance of Ca^{2+} -binding proteins in plasma. Moreover, 2x collapsing buffer was used to overcome the intrinsic buffering capacity of the plasma and maintain the pH at 4.5. Figure 3 shows that up to 80% of the target iLOV-Doc protein could be recovered from 10% plasma following magnetic processing with pNIPAm-mNPs. At iLOV-Doc concentrations higher than 1 μ M, the capture efficiency decreased slightly to >70%. These findings demonstrate the capability of the pNIPAm-mNPs/ELP-Coh system for specific capture of the target protein in biological samples at an appropriate dilution. The same samples that were processed and quantified for iLOV-Doc fluorescence were also analyzed using SDS-PAGE (Figure 3B) which showed that the majority of the background plasma proteins were removed following magnetic processing. Magnetic separation of ELP-Coh was found to be especially effective at removing large molecular

weight plasma proteins, while some albumin was nonspecifically captured and transferred together with iLOV-Doc. Fluorescence imaging of iLOV-Doc fluorescence in the SDS-PAGE gel is shown in the bottom of Figure 3B.

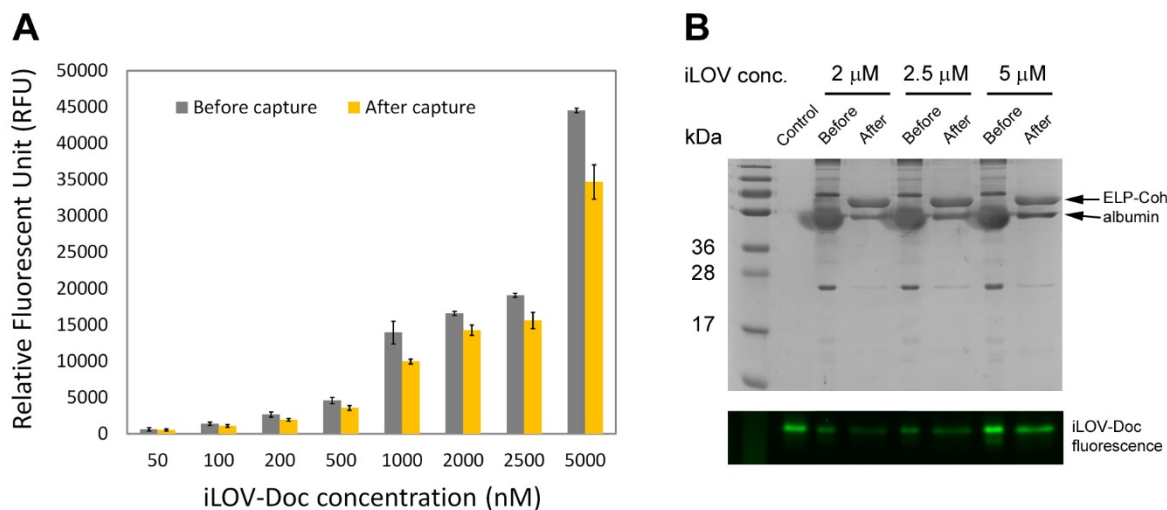


Figure 3. Capture of iLOV-Doc in diluted human plasma. **(A)** Fluorescent intensity of iLOV-Doc measured before capture in TBS-Ca + 10% human blood plasma, and after capture in releasing buffer. The fluorescence intensity was blanked by subtracting the intensity of pure buffer or buffer + 10% human blood plasma. **(B)** SDS-PAGE gel and fluorescent visualization of samples with different iLOV-Doc concentrations before and after capture. Pure iLOV-Doc (5 μ M) in clean buffer was used as control.

To test cell capture, we created a yeast model displaying Doc fusion proteins by cloning GFP-Doc or iLOV-Doc genes into a pYD1 yeast display plasmid. Expression levels were found to be slightly higher for GFP-Doc, and so only GFP-Doc was used for further testing, although both cell types were successfully captured by the pNIPAm-mNPs and ELP-Coh (Figure S4, panel A-C). Display of GFP-Doc through the Aga1p-Aga2p system was complete 40 hours post-induction. Antibody staining for the XPress-tag located between the Aga2p domain and the GFP-Doc showed

that approximately 60% of the cell population was positive for display on the outer cell wall (Figure S4, panel D, Supporting information), which is a typical percentage of cells successfully induced using this display system.⁴³ For cell capture experiments, the highest achievable fraction of GFP-Doc positive cells was therefore 60%. We added ELP-Coh and pNIPAm-mNPs into cell suspensions, triggered the phase separation with collapsing buffer, and separated the aggregates with a magnet (Figure 4A). Three fractions (Sup1, Wash, Sup2) were collected and analyzed with flow cytometry. The results in Figure 4B (left panel) showed that ~50 - 60% of non-displaying (wild-type) cells were removed in the non-captured Sup1 and Wash fractions, while approximately 71.4 % of the GFP-Doc target cells were captured.

In order to demonstrate the ability of the pNIPAm-mNPs and ELP-Coh system to specifically capture target cells with low abundance in a heterogeneous population, serial dilutions of the GFP-Doc-displaying cells were prepared by addition of wild-type negative yeast cells while maintaining the total cell number at $\sim 6.25 \times 10^6$ cells/mL for binding with the ELP-Coh prior to magnetic separation. The cell capture experiments were first conducted in clean buffer. Capture of the GFP-Doc displaying cells was performed using collapsing buffer and magnetic separation. The captured cell fractions were then analyzed using flow cytometry. The cell capture efficiency and the enrichment factors were plotted in Figure 4C (left panel) as a function of the fraction GFP-Doc positive cells in the original sample. For samples with a GFP-Doc positive cell fraction <15%, we found the highest capture efficiencies of up to ~100%, e.g. for a starting sample with 1% GFP-positive cells. In addition, the target cell population could be enriched by a factor up to 2.5, especially for samples with a low fraction of GFP-Doc target cells. Capture efficiency and enrichment factor subsequently decreased with a higher percentage of GFP-positive cells (>15%) (Figure S6, Supporting information).

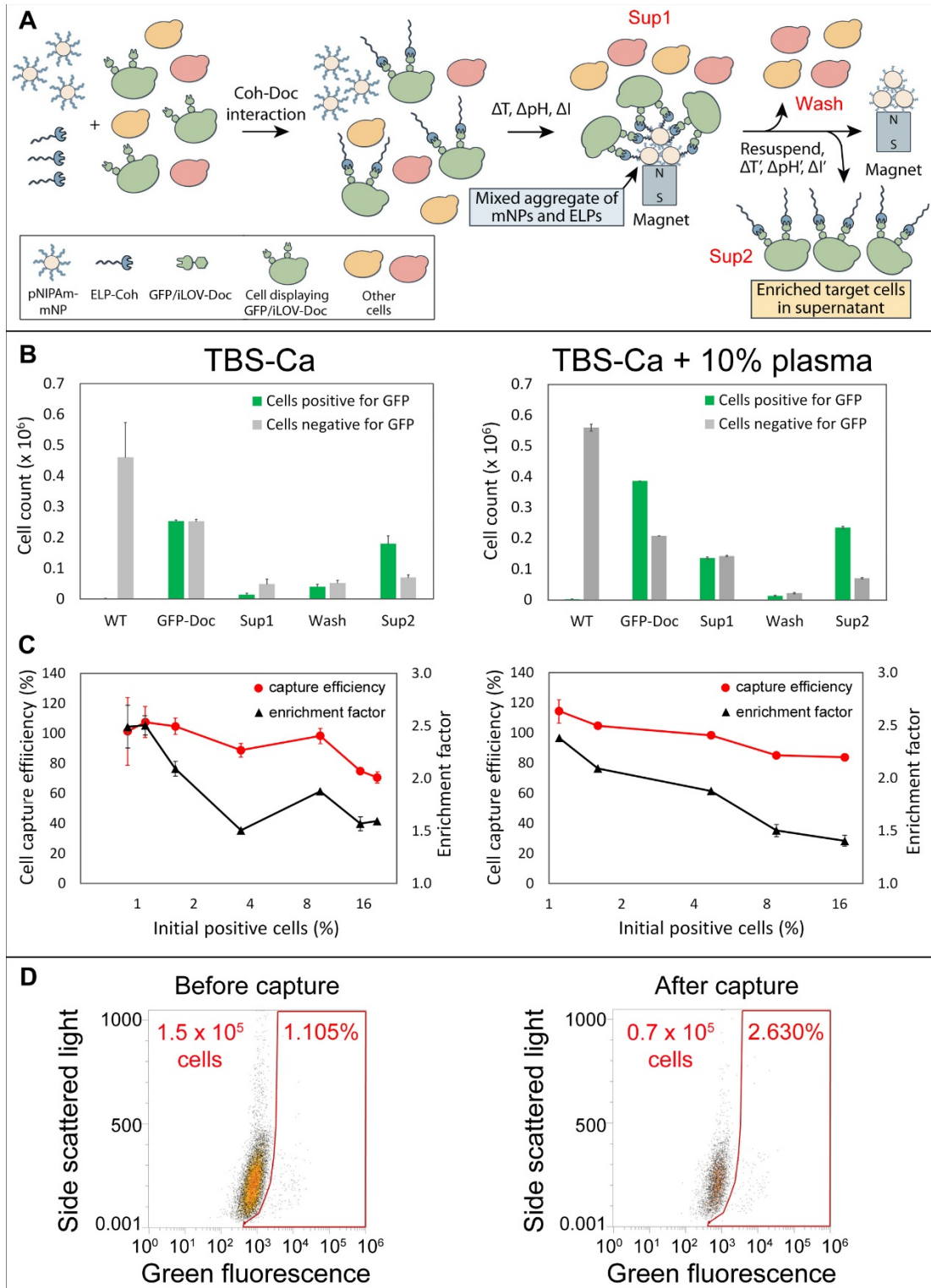


Figure 4. Capture of yeast cells displaying GFP-Doc using pNIPAm-mNPs/ELP-Coh system. (A)

Scheme depicting reagent system for specific capture and magnetic separation of yeast cells

displaying GFP-Doc. The magnetophoretic procedure has four steps as described for capturing free iLOV-Doc. **(B)** GFP-Doc positive and negative cell count in different fractions after separation. The non-captured cells were collected in 'Sup1' and 'Wash' fractions using collapsing buffer, whereas the captured cells were obtained with releasing buffer in the 'Sup2' fraction. Non-displaying wild-type (WT) cells were used as a negative control. **(C)** Cell capture efficiency and enrichment factor for target cells at different abundance levels. For figures B and C, the left panels show samples prepared in TBS-Ca buffer, while the right panels show samples prepared in TBS-Ca buffer supplemented with 10% human blood plasma. **(D)** Flow-cytometry results for a sample with approximately ~1.1% target cells in the original sample (defined by the red gate). After capture and separation by the pNIPAm-mNPs/ELP-Coh system, analytical flow cytometry demonstrated a capture efficiency of ~100% as well as a 2.4-fold enrichment of target cells above the background, while the number of non-displaying negative cells was reduced by more than 50%.

To mimic a more realistic clinical sample matrix, we utilized the pNIPAm-mNPs/ELP-Coh system for capturing cells from diluted 10% human plasma, resulting in similar capture efficiencies (Figure 4B, C right panels). The pNIPAm-mNPs/ELP-Coh system thus showed specificity for binding to GFP-Doc displayed on the yeast cell wall in the presence of high levels of plasma proteins. For capturing cells from dilute plasma, the same modifications to the collapsing conditions were applied as were done for capturing free iLOV-Doc in diluted plasma sample (i.e., increased Ca^{2+} and increased collapsing buffer concentration). A representative cell capture result from 10% plasma is shown in Figure 4D in which a starting sample ($\sim 6.25 \times 10^6$ cells/mL of TBS + 10% plasma) containing ~1.1% GFP-Doc displaying cells was subjected to magnetophoresis

using the pNIPAm-mNPs/ELP-Coh system. The captured cells were suspended into the same volume. In this case, ~90% of the GFP-Doc cells were captured and the percentage of these cells in the resulting population was increased to ~2.6% (2.4-fold enrichment). When viewed from the point of view of the background cells, about 1.5×10^5 /mL GFP-Doc negative cells were in the original sample, while in the Sup2 fraction, this number was reduced to 0.7×10^5 /mL, representing removal of more than 50% background cells.

Minimizing non-specific carryover of target molecules and cells is a challenge for smart polymer-based affinity separations, as is the case for all bioseparation systems. We noticed carryover of BSA (or human serum albumin) when capturing and enriching free iLOV-Doc from buffers and diluted plasma (Figure 2D and 3B), as well as a ~50% carryover of GFP-Doc negative cells (Figure 4D) that were separated along with GFP-Doc displaying cells. This nonspecific carryover is attributed to hydrophobic interactions between background proteins and pNIPAm-mNPs/ELP aggregates, while in the case of cellular capture, physical entanglement of cells inside pNIPAm-mNPs/ELP-Coh aggregates is thought to be the cause. Despite these limitations, specificity of binding and capturing was still found to be rapid and robust. Additionally, our presented systems has improved simplicity as compared to classical magnetic separation process. Our system eliminates both the requirement for bioconjugation of any receptors to nanoparticles and eliminates the centrifugal separation step. These combined advantages make it feasible and attractive among existing immunoseparation techniques.⁴⁴ We further note that the system as presented is compatible with many other molecular binders (e.g. antibodies, aptamers, nucleic acids) for targeting any molecular target of choice.

From the data of the capture experiments for iLOV-Doc and yeast cells displaying GFP-Doc in diluted human blood plasma samples (Figure 3 and Figure S6B, Supporting information),

representative calibration curves for detection of these targets were generated (Figure S7, Supporting information) and the detection limits were determined as 311.2 nM (for free iLOV-Doc) and 0.38×10^6 cells/mL (for yeast cells displaying GFP-DocI).

Conclusively, we have presented a new system for magnetic capture, separation and enrichment of molecular and cellular targets based on co-aggregation between pNIPAm-mNPs and ELP fusion proteins. We demonstrate for the first time magnetic actuation of ELPs with a system that has the advantages of being rapid, robust, and compatible with point-of-care assays. Our system eliminates the requirement of modifying the magnetic nanoparticle surface with affinity biomolecules of any kind, and allows for production of pNIPAm-mNPs *en masse* without any further post-synthesis derivatization. The protein capture reagent (in our case, Coh) is produced as a genetic fusion with an appropriately designed ELP, and can be purified in a functional form using a chromatography-free thermo-precipitation method. This workflow means large amounts of both the magnetic nanoparticles and biofunctional capture reagents can be obtained without the need for chromatography, or post-synthesis modification. In addition to providing a fundamentally new approach to magnetic bioseparations, our system effectively streamlines the material-production requirements for a wide range of magnetic separations and cell capture applications. We anticipate that in the near future, this line of research involving aggregate formation between nanoparticles bearing pNIPAm and affinity proteins (e.g. antibodies) bearing ELPs will provide significant opportunities in the areas of bioseparations, drug delivery, and *in vivo* imaging.

ASSOCIATED CONTENT

Supporting Information. The Supporting Information is available free of charge on the ACS Publications website at DOI:.

Experimental details (synthesis of the pNIPAm and pNIPAm-mNPs; cloning, expression and purification of the ELP-Coh, iLOV-Doc and Coh-iLOV; LCST determination for the mNPS and ELP-Coh; preparation of yeast cells displaying GFP/iLOV-Doc; co-aggregation of the pNIPAm-mNPs and ELP-Coh and its use for capturing iLOV-Doc or cells displaying GFP-Doc), amino acid sequences of all proteins, as well as additional figures (SDS-PAGE, SEC and flow cytometric data) (PDF).

AUTHOR INFORMATION

Corresponding Authors

*E-mail: michael.nash@unibas.ch

Tel: +41 61 207 38 44

ORCID:

Duy Tien Ta: 0000-0002-3901-638X

Notes

The authors declare no competing financial interest.

ACKNOWLEDGMENTS

The authors kindly thank the National Centre of Competence in Research: Molecular Systems Engineering (NCCR-MSE) and the Human Frontier Science Program (HFSP) Young Investigator Grant (RGY80/2015) for financially funding this research.

REFERENCES

- (1) Pankhurst, Q. A.; Connolly, J.; Jones, S. K.; Dobson, J. J. *Phys. D Appl. Phys.* **2003**, *36*, R167.
- (2) Ito, A.; Shinkai, M.; Honda, H.; Kobayashi, T. *J. Biosci. Bioeng.* **2005**, *100*, 1–11.
- (3) Ranzoni, A.; Sabatte, G.; van Ijzendoorn, L. J.; Prins, M. W. J. *ACS Nano* **2012**, *6*, 3134–3141.
- (4) Sapsford, K. E.; Algar, W. R.; Berti, L.; Gemmill, K. B.; Casey, B. J.; Oh, E.; Stewart, M. H.; Medintz, I. L. *Chem. Rev.* **2013**, *113*, 1904–2074.
- (5) Lai, J. J.; Hoffman, J. M.; Ebara, M.; Hoffman, A. S.; Estournès, C.; Wattiaux, A.; Stayton, P. S. *Langmuir* **2007**, *23*, 7385–7391.
- (6) Lai, J. J.; Nelson, K. E.; Nash, M. A.; Hoffman, A. S.; Yager, P.; Stayton, P. S. *Lab Chip* **2009**, *9*, 1997.
- (7) Nehilla, B. J.; Hill, J. J.; Srinivasan, S.; Chen, Y.-C.; Schulte, T. H.; Stayton, P. S.; Lai, J. *J. Anal. Chem.* **2016**, *88*, 10404–10410.
- (8) Nash, M. A.; Waitumbi, J. N.; Hoffman, A. S.; Yager, P.; Stayton, P. S. *ACS Nano* **2012**, *6*, 6776–6785.
- (9) Nash, M. A.; Yager, P.; Hoffman, A. S.; Stayton, P. S. *Bioconjug. Chem.* **2010**, *21*, 2197–2204.
- (10) Nash, M. A.; Lai, J. J.; Hoffman, A. S.; Yager, P.; Stayton, P. S. *Nano Lett.* **2010**, *10*, 85–91.
- (11) Narain, R.; Gonzales, M.; Hoffman, A. S.; Stayton, P. S.; Krishnan, K. M. *Langmuir* **2007**, *23*, 6299–6304.
- (12) Sonti, S. V.; Bose, A. *J. Colloid Interface Sci.* **1995**, *170*, 575–585.

- (13) Pamme, N.; Wilhelm, C. *Lab Chip* **2006**, *6*, 974–980.
- (14) Xu, H.; Aguilar, Z. P.; Yang, L.; Kuang, M.; Duan, H.; Xiong, Y.; Wei, H.; Wang, A. *Biomaterials* **2011**, *32*, 9758–9765.
- (15) Molday, R. S.; MacKenzie, D. *J. Immunol. Methods* **1982**, *52*, 353–367.
- (16) Fierer, J. O.; Veggiani, G.; Howarth, M. *Proc. Natl. Acad. Sci. U. S. A.* **2014**, *111*, E1176–E1181.
- (17) Boyer, C.; Whittaker, M. R.; Bulmus, V.; Liu, J. *NPG Asia* **2010**.
- (18) Mehta, R. V.; Upadhyay, R. V.; Charles, S. W.; Ramchand, C. N. *Biotechnology* **1997**, *11*, 493–496.
- (19) Koh, I.; Wang, X.; Varughese, B.; Isaacs, L.; Ehrman, S. H.; English, D. S. *J. Phys. Chem. B* **2006**, *110*, 1553–1558.
- (20) Steen Redeker, E.; Ta, D. T.; Cortens, D.; Billen, B.; Guedens, W.; Adriaensens, P. *Bioconjug. Chem.* **2013**, *24*, 1761–1777.
- (21) Van Leemputten, E. and Horisberger, M. *Biotechnol. Bioeng.* **1974**, *16*, 385–396.
- (22) Kazenwadel, F.; Wagner, H.; Rapp, B. E.; Franzreb, M. *Anal. Methods* **2015**, *7*, 10291–10298.
- (23) Marciello, M.; Filice, M.; Olea, D.; Velez, M.; Guisan, J. M.; Mateo, C. *Langmuir* **2014**, *30*, 15022–15030.
- (24) Danczyk, R.; Krieder, B.; North, A.; Webster, T.; HogenEsch, H.; Rundell, A. *Biotechnol. Bioeng.* **2003**, *84*, 215–223.
- (25) Chen, G. H.; Hoffman, A. S. *Bioconjug. Chem.* **1993**, *4*, 509–514.
- (26) Ding, Z. L.; Chen, G. H.; Hoffman, A. S. *Bioconjug. Chem.* **1996**, *7*, 121–125.

- (27) Heredia, K. L.; Bontempo, D.; Ly, T.; Byers, J. T.; Halstenberg, S.; Maynard, H. D. *J. Am. Chem. Soc.* **2005**, *127*, 16955–16960.
- (28) Matsumoto, N. M.; Prabhakaran, P.; Rome, L. H.; Maynard, H. D. *ACS Nano* **2013**, *7*, 867–874.
- (29) Golden, A. L.; Battrell, C. F.; Pennell, S.; Hoffman, A. S.; J Lai, J.; Stayton, P. S. *Bioconjug. Chem.* **2010**, *21*, 1820–1826.
- (30) Chua, G. B. H.; Roth, P. J.; Duong, H. T. T.; Davis, T. P.; Lowe, A. B. *Macromolecules* **2012**, *45*, 1362–1374.
- (31) Moatsou, D.; Li, J.; Ranji, A.; Pitto-Barry, A.; Ntai, I.; Jewett, M. C.; O'Reilly, R. K. *Bioconjug. Chem.* **2015**, *26*, 1890–1899.
- (32) Meyer, D. E.; Chilkoti, A. *Nat. Biotechnol.* **1999**, *17*, 1112–1115.
- (33) Shu, J. Y.; Panganiban, B.; Xu, T. *Annu. Rev. Phys. Chem.* **2013**, *64*, 631–657.
- (34) Gibson, M. I.; O'Reilly, R. K. *Chem. Soc. Rev.* **2013**, *42*, 7204–7213.
- (35) Moatsou, D.; Li, J.; Ranji, A.; Pitto-Barry, A.; Ntai, I.; Jewett, M. C.; O'Reilly, R. K. *Bioconjug. Chem.* **2015**, *26*, 1890–1899.
- (36) Kowalczyk, T.; Hnatuszko-Konka, K.; Gerszberg, A.; Kononowicz, A. K. *World J. Microbiol. Biotechnol.* **2014**, *30*, 2141–2152.
- (37) Stahl, S. W.; Nash, M. A.; Fried, D. B.; Slutzki, M.; Barak, Y.; Bayer, E. A.; Gaub, H. E. *Proc. Natl. Acad. Sci. U. S. A.* **2012**, *109*, 20431–20436.
- (38) Nash, M. A.; Smith, S. P.; Fontes, C. M.; Bayer, E. A. *Curr. Opin. Struct. Biol.* **2016**, *40*, 89–96.
- (39) Jobst, M. A.; Schoeler, C.; Malinowska, K.; Nash, M. A. *J. Vis. Exp.* **2013**, *82*, e50950.

- (40) Kamezaki, Y.; Enomoto, C.; Ishikawa, Y.; Koyama, T.; Naya, S.-I.; Suzuki, T.; Sakka, K. *Protein Expr. Purif.* **2010**, *70* (1), 23–31.
- (41) Jones, S. T.; Walsh-Korb, Z.; Barrow, S. J.; Henderson, S. L.; del Barrio, J.; Scherman, O. A. *ACS Nano* **2016**, *10*, 3158–3165.
- (42) Chapman, S.; Faulkner, C.; Kaiserli, E.; Garcia-Mata, C.; Savenkov, E. I.; Roberts, A. G.; Oparka, K. J.; Christie, J. M. *Proc. Natl. Acad. Sci. U. S. A.* **2008**, *105*, 20038–20043.
- (43) Boder, E. T.; Wittrup, K. D. *Nat. Biotechnol.* **1997**, *15*, 553–557.
- (44) Zborowski, M.; Chalmers, J. J. *Magnetic Cell Separation*; Elsevier, 2008.
- (45) Otten, M.; Ott, W.; Jobst, M. A.; Milles, L.; Verdorfer, T.; Pippig, D.; Nash, M. A.; Gaub, H. E. *Nat. Methods* 2014, *11*, 1127–1130.

For TOC only

